

# Thermodynamics and Mechanism of the Block Copolymer Micelle Shuttle between Water and an Ionic Liquid

Zhifeng Bai<sup>†</sup> and Timothy P. Lodge<sup>\*,†,‡</sup>

Department of Chemistry and Department of Chemical Engineering and Materials Science, University of Minnesota, Minneapolis, Minnesota 55455

Received: July 24, 2009; Revised Manuscript Received: August 20, 2009

The micelle shuttle utilizing block copolymer micelles as nanocarriers for transportation between water and a hydrophobic ionic liquid, 1-ethyl-3-methylimidazolium bis(trifluoromethylsulfonyl)imide ([EMIM][TFSI]), is examined in detail. Rhodamine B, a dye with a high molar absorptivity and fluorescence quantum yield, is conjugated to a short poly(1,2-butadiene) homopolymer and then loaded in amphiphilic poly((1,2-butadiene)-block-ethylene oxide) (PB–PEO) block copolymer micelles. The round-trip transportation of the micelles between water and the ionic liquid is simply triggered by temperature; it is fully reversible, quantitative, and without leakage. Quantitative fluorescence analysis reveals that the micelle distribution in the biphasic system has a very strong temperature dependence, which is favorable for control of the transportation. The standard Gibbs free energy change ( $\Delta G^\circ$ ), standard enthalpy change ( $\Delta H^\circ$ ), and standard entropy change ( $\Delta S^\circ$ ) of the micelle shuttle are extracted from the temperature dependence of the micelle distribution. Both  $\Delta H^\circ$  and  $\Delta S^\circ$  are positive, indicating an entropy-driven process. The slow yet spontaneous micelle shuttle is explored under quiescent conditions to understand the transfer kinetics. Both of the two-way transfers involve three steps, formation of micelle-concentrated [EMIM][TFSI]/water droplets in the initial phase, sedimentation/creaming of the droplets to the interface, and diffusion of the micelles to the destination phase. A detailed mechanism for the transfer is therefore proposed.

## Introduction

Block copolymer micelles are of great interest as encapsulators and nanocarriers in diverse applications, including delivery,<sup>1</sup> separations,<sup>2</sup> and catalysis.<sup>3</sup> When amphiphilic block polymers self-assemble in a selective solvent, the insoluble blocks pack into a dense core that is shielded by the corona of soluble blocks.<sup>4</sup> The core–corona structure allows solubilization and transport of cargo molecules in an otherwise inhospitable environment. The size, morphology, stability, and functionality of the micelles can be tuned by various block copolymer attributes, such as molecular weight, composition, structure, and monomer choice.<sup>5</sup> Solvent quality is another important parameter to tune the structure.<sup>6</sup>

Ionic liquids are molten salts with melting points below room temperature. Due to their attractive features, including negligible volatility, widely tunable solvation properties, and good chemical and thermal stability, they are extensively explored as media for reactions and separations.<sup>7</sup> Micellization in ionic liquids can impart desirable nanostructures, which may expand or enhance the applications of ionic liquids, such as solubilization of ionic-liquid-phobic substances and preparation of nanomaterials in ionic liquids.<sup>8</sup> Certain surfactants also show self-assembly into micelles in ionic liquids.<sup>9</sup> Micellization of block copolymers in ionic liquids<sup>10,11</sup> is an exciting emerging area.<sup>12</sup> For example, poly((1,2-butadiene)-block-ethylene oxide) (PB–PEO) block copolymers adopt the canonical micelle structures—spheres, cylinders, and vesicles—in the ionic liquid 1-butyl-3-methylimidazolium hexafluorophosphate ([BMIM][PF<sub>6</sub>]), and their structures are temperature-independent from 25 to 100 °C.<sup>10a</sup> Also,

a micellization–unimer–inverse micellization morphology sequence was realized by a doubly thermosensitive poly(benzyl methacrylate-block-N-isopropylacrylamide) (PBnMA–PNIPAm) block copolymer in 1-ethyl-3-methylimidazolium bis(trifluoromethylsulfonyl)imide ([EMIM][TFSI]);<sup>10c</sup> PBnMA<sup>13</sup> and PNIPAm<sup>14</sup> have a lower critical solution temperature (LCST) phase behavior, i.e., solubility decreases with increasing temperature, and an upper critical solution temperature (UCST) phase behavior, respectively, which are more typically observed in water solutions and organic solutions, respectively.

The micelle shuttle is an interesting phenomenon in which PB–PEO block copolymer micelles transfer from an aqueous phase at room temperature to a hydrophobic ionic liquid at elevated temperature.<sup>15</sup> The transfer is fully reversible and can be repeated many times. The micelle structures are preserved during the transfer without substantial micellar reorganization, which is consistent with the kinetically trapped structures of the highly amphiphilic PB–PEO micelles in both water<sup>16</sup> and ionic liquids.<sup>10a,d</sup> We have further shown that the driving force of the micelle shuttle originates from the LCST phase behavior of PEO in water, and hence, the transfer temperature can be effectively tuned by adding additives to the water phase to adjust the LCST of PEO.<sup>17</sup> To control the loading and release in the micelle shuttle, we have developed a fully thermoreversible micellization–transfer–demicellization shuttle between water and an ionic liquid by using a multithermosensitive PNIPAm–PEO block copolymer, in which the PNIPAm core block is doubly and inversely thermosensitive in water and the ionic liquid.<sup>18</sup> An analogous micelle shuttle system with poly(oxazoline) block copolymers was also reported recently.<sup>19</sup> Such a simple round-trip delivery system could enable straightforward recovery of valuable payloads, such as catalysts.<sup>20</sup> In particular, since ionic liquids are attractive as reaction media yet they are

\* Author for correspondence. E-mail: lodge@umn.edu.

<sup>†</sup> Department of Chemistry.

<sup>‡</sup> Department of Chemical Engineering and Materials Science.

**TABLE 1: Molecular Characteristics of Polymers**

polymer <sup>a</sup>	$M_{\text{PB}}^b$ (kg mol <sup>-1</sup> )	$M_{\text{PEO}}^b$ (kg mol <sup>-1</sup> )	PDI <sup>c</sup>	$f_{\text{PEO}}^d$
PB-PEO(4-7)	3.6	6.5	1.07	0.58
PB <sup>e</sup>	2.0			1.11

<sup>a</sup> 90% 1,2-addition of PB block microstructures determined by <sup>1</sup>H NMR.

<sup>b</sup> Number-average molecular weight determined by <sup>1</sup>H NMR.

<sup>c</sup> Polydispersity index (PDI) determined by size exclusion chromatography (SEC).

<sup>d</sup> Volume fraction of PEO block determined by <sup>1</sup>H NMR and the amorphous densities of PB and PEO,  $\rho_{\text{PB}} = 0.87 \text{ g cm}^{-3}$  and  $\rho_{\text{PEO}} = 1.13 \text{ g cm}^{-3}$ , respectively (see ref 26).

<sup>e</sup> Quantitative hydroxyl termination yield determined by <sup>1</sup>H NMR.

relatively expensive and their toxicity is still unclear, it could be desirable to utilize the micelle shuttle to transport nonpolar reagents or products quantitatively into or out of an ionic liquid reaction medium via an immiscible stream, whereby the water phase can be used for product recovery while the ionic liquid remains in its reaction vessel for repeated usage. Indeed, liquid–liquid biphasic systems containing ionic liquids as one phase have shown significant promise in biphasic catalysis.<sup>21</sup> Related microemulsion<sup>22</sup> and emulsion<sup>23</sup> systems containing ionic liquids are also of great interest in fundamental research and practical applications.

Herein, we examine the transportation capability of the micelle shuttle by using dye-loaded micelles, and further take advantage of the dye visibility to study the transfer mechanism in detail. Since organic dyes are generally somewhat or greatly soluble in ionic liquids,<sup>24</sup> we chose to couple a dye with a nonpolar PB homopolymer to achieve low dye solubility in both solvents, and favorable dye loading in the micelle cores. Rhodamine B was chosen as the dye due to its large molar absorptivity and fluorescence quantum yield.<sup>25</sup> The transport and partitioning of the micelle shuttle was clearly visualized by the strong absorption and emission of the dye loaded in the micelles. Fluorescence analysis was applied to quantify the temperature dependence of the micelle distribution in the biphasic system, an important parameter of the transportation. Further efforts were exerted to understand the transfer thermodynamics and kinetics, and a detailed transfer mechanism for the micelle shuttle is proposed.

## Experimental Section

**Materials.** A PB-PEO block copolymer, prepared by Dr. Kevin P. Davis, and a hydroxyl-terminated PB homopolymer were synthesized via anionic polymerization as previously reported.<sup>27</sup> The molecular characteristics of the polymers are summarized in Table 1. [EMIM][TFSI] was prepared via a synthetic route reported previously.<sup>28</sup> This clear and colorless liquid was used after drying in a vacuum oven at ~60 °C for 3 days. Rhodamine B base, phosphorus oxychloride, 1,2-dichloroethane, and anhydrous pyridine were obtained from Sigma-Aldrich and used as received.

**General Methods.** <sup>1</sup>H NMR spectra were obtained on a Varian Inova 500 MHz spectrometer. SEC measurements were taken on a system equipped with a Wyatt DAWN DSP multiangle light scattering detector, a Wyatt OPTILAB DSP refractive index detector, and three Phenogel (Phenomenex) columns. Tetrahydrofuran (THF) was used as the eluent. Absorption spectra of dye-loaded micelle solutions were acquired on a Varian Cary 100Bio UV-visible spectrophotometer using pristine micelle solutions without dye loading as references. Fluorescence spectra were measured on a Varian Cary Eclipse fluorescence spectrophotometer at an excitation wave-

length of 510 nm, with excitation and emission slits of 10 nm. All of the samples were kept at 4 °C in a refrigerator and thermally stabilized at 10.0 °C ( $\pm 0.1$  °C) by a temperature controller prior to measurements. Matrix-assisted laser desorption/ionization time-of-flight (MALDI-TOF) mass spectrometry experiments were collected on a Bruker Reflex III instrument equipped with a nitrogen laser (337 nm), a delayed extraction Scout ion source, a high-resolution multichannel plate (MCP) detector in the reflector mode, and a 2 GHz digitizer. THF solutions of matrix (dithranol, 20 mg/mL), cationizing agent (silver trifluoroacetate, 2 mg/mL), and polymer (10 mg/mL) were mixed with a ratio of 15:3:5. Dynamic light scattering (DLS) was performed on a homemade photometer as previously reported.<sup>17</sup>

**Synthesis and Characterization of Rhodamine B-Poly(1,2-butadiene) (Rho-PB).** To synthesize rhodamine B acid chloride, phosphorus oxychloride (0.6 mL) was added dropwise to a solution of rhodamine B base (1.0 g, 2.3 mmol) in 1,2-dichloroethane (12 mL) under stirring over 5 min. The solution was refluxed for 4 h. The reaction mixture was cooled, and volatiles were evaporated in vacuo to give rhodamine B acid chloride. Quantitative conversion was confirmed by <sup>1</sup>H NMR,<sup>29</sup> and the product was used without further purification. Rho-PB was synthesized by coupling rhodamine B acid chloride with the hydroxyl-terminated PB.<sup>30</sup> To a THF solution (20 mL) of the hydroxyl-terminated PB (0.75 g), rhodamine B acid chloride (2 M excess) and anhydrous pyridine (0.5 mL) were added in a high-pressure glass reactor under an argon atmosphere. The reactor was sealed and heated at 40 °C for 3 days. The reaction was terminated with methanol (2 mL), and volatiles were evaporated in vacuo. The residue was diluted with dichloromethane, precipitated in cold methanol in a dry ice/isopropanol bath, and washed with cold methanol. The coupling was confirmed by MALDI-TOF mass spectrometry (Figure S1 in the Supporting Information).<sup>30</sup> <sup>1</sup>H NMR analysis yielded a coupling yield of ~50%.

**Solution Preparation.** For Rho-PB-loaded PB-PEO micelle solutions, the concentration of the PB-PEO(4-7) block copolymer was 0.5 wt % and the molar ratio of the block copolymer to Rho-PB was 5:2. For dye loading in water, the block copolymer and Rho-PB were first dissolved in dichloromethane. The solvent was removed by a gentle nitrogen purge and then heating at ~60 °C in a vacuum oven overnight. The resulting well-mixed thin film was hydrated by water and stirred at room temperature for 1 week. The solution was filtered through a 0.45 μm PTFE syringe filter and subsequently dialyzed in a membrane tube with a molecular weight cutoff of 10 000 against water. For dye loading in [EMIM][TFSI], the block copolymer, Rho-PB, and [EMIM][TFSI] were mixed with a dichloromethane cosolvent until complete dissolution. Most of the cosolvent was slowly removed by a gentle nitrogen purge, and the solution was dried at ~60 °C in a vacuum oven until constant weight was achieved. To remove unloaded Rho-PB, water was added to the [EMIM][TFSI] solution. The dye-loaded PB-PEO micelles transferred to the aqueous phase while the unloaded Rho-PB remained in the [EMIM][TFSI] phase. The aqueous phase was taken out and added to fresh [EMIM][TFSI]. Upon heating, the micelles transferred back to the [EMIM][TFSI] phase, which was then taken out and dried at ~60 °C in a vacuum oven until a constant weight was achieved. We estimate the average number of dyes per micelle to be 40. The dye-loaded micelle solutions were

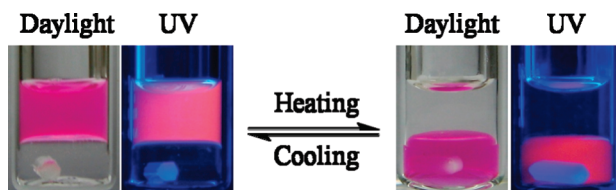


**Figure 1.** Images of the dye-loaded micelle shuttle between water (the upper phase) and [EMIM][TFSI] (the lower phase). The system was irradiated separately by daylight lamps and a UV lamp with a wavelength of 365 nm. The images were taken at 25 °C (left) and 70 °C (right).

diluted to appropriate concentrations for the micelle shuttle studies described below.

THF solutions of Rho-PB were prepared by consecutive dilution of a 10 M<sup>-4</sup> stock solution. Cold THF was used during the dilution.

**Micelle Shuttle.** For consistency, the dye-loaded micelles were initially prepared in [EMIM][TFSI] for the thermodynamic and kinetic studies. For the measurement of the temperature dependence of the micelle distribution, a biphasic micelle shuttle system (8 mL for each phase) was equilibrated at room temperature in a 25 mL glass flask. The system was sealed and placed in a silicon oil bath and then heated to each of 10 temperatures from 25 to 65 °C ( $\pm 0.1$  °C) with rapid stirring. The system was equilibrated for 12 h at temperatures between 50 and 57 °C and for 4 h at the other temperatures. Aliquots (0.2 mL) of both phases were separately and carefully taken out by syringes and then diluted by THF to 15 times by volume, in which the dilution was scaled by weight in terms of the densities of water, [EMIM][TFSI], and THF.

For the transfer of the dye-loaded micelles from water to [EMIM][TFSI] under quiescent conditions upon heating, a glass vial containing the equilibrated biphasic system at room temperature was placed into a preheated silicon oil bath and heated without disturbance. For the micelle transfer from [EMIM][TFSI] to water under quiescent conditions upon cooling the micelle shuttle system previously equilibrated at high temperature, the silicon oil bath heating the equilibrated system at high temperature was removed and the system was cooled without disturbance to room temperature ( $22 \pm 1$  °C). For the micelle transfer from [EMIM][TFSI] to water under quiescent conditions at room temperature, water was carefully added to a dry [EMIM][TFSI] solution of the micelles at room temperature, without stirring.

## Results and Discussion

**The Dye-Loaded Micelle Shuttle.** Rhodamine B–poly(1,2-butadiene) (Rho-PB) is insoluble in water and very sparingly soluble in [EMIM][TFSI]. However, it can be effectively solubilized by loading into the PB–PEO micelles in both water and [EMIM][TFSI] (Figure S2 in the Supporting Information). Dye-loaded micelles prepared in both water and [EMIM][TFSI] exhibit the micelle shuttle; Figure 1 shows representative experimental images. The partitioning of the micelles can be readily visualized by the strong absorption and emission of the dye; the micelles prefer the aqueous phase at room temperature but transfer to the ionic liquid phase upon heating to 70 °C. Cooling the system back to room temperature induces the reverse transfer. The transfer is quantitative (see below), without leakage of the “payload”, and can be repeated many times.

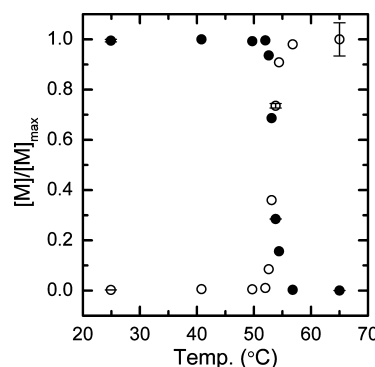


**Figure 2.** Temperature dependence of normalized micelle concentrations in the aqueous phase (filled) and the ionic liquid phase (open) in the micelle shuttle.

**Temperature Dependence of Micelle Distribution.** For transportation using the micelle shuttle, it is important to quantify the temperature dependence of the micelle distribution in the biphasic system. Rhodamine B with very high molar absorptivity and fluorescence quantum yield is quite suitable for the quantitative analysis.<sup>25</sup> The fluorescence intensity of Rho-PB is linear with a concentration over at least 3 orders of magnitude (Figure S4 in the Supporting Information), indicating the feasibility of the analysis. Figure 2 shows the temperature dependence of the normalized micelle concentration ([M]/[M]<sub>max</sub>) in the aqueous phase and the ionic liquid phase, where the micelle concentrations are obtained from the fluorescence intensity of Rho-PB loaded in the micelles. The micelle distribution in the biphasic system has a very strong temperature dependence and the transfer happens over a narrow window, indicated by a sharp decrease of the micelle concentration in the aqueous phase beginning at  $\sim 52$  °C and simultaneously a sharp increase in the ionic liquid phase. For example, 99.6% of the micelles are in the aqueous phase at 52.0 °C, but only 0.3% remain at 56.8 °C (Table 2). This strong temperature dependence of the micelle distribution is advantageous for precise control of round-trip quantitative transport by the micelle shuttle.

**Thermodynamics of Transfer.** Important thermodynamic variables of the micelle shuttle can be extracted from the temperature dependence of the micelle distribution. Assuming that the mean aggregation number of the micelles does not change in the transfer and that it is independent of temperature, which is supported by our previous results,<sup>15,17</sup> and is consistent with these kinetically stable micelles in both water<sup>6b,16</sup> and the ionic liquid,<sup>10d,17</sup> the micelle shuttle can be expressed as an equivalent equilibrium

$$M_{aq} \rightleftharpoons M_{IL} \quad (1)$$

The equilibrium constant (*K*) at a given temperature can therefore be written as

$$K = \frac{[M]_{IL}}{[M]_{aq}} \quad (2)$$

where [M]<sub>aq</sub> and [M]<sub>IL</sub> are the micelle concentrations in the aqueous phase and the ionic liquid phase, respectively, and can be calculated by the normalized micelle concentration values in Table 2.<sup>31</sup> Then, the standard Gibbs free energy change ( $\Delta G^\circ$ ),

**TABLE 2: Temperature Dependence of the Normalized Micelle Concentrations in the Aqueous Phase and the Ionic Liquid Phase, the Equilibrium Constant, and the Standard Gibbs Free Energy Change per Mole of Micelles in the Micelle Shuttle<sup>a</sup>**

temp (°C)	24.9	40.8	49.7	52.0	52.6
[M] <sub>aq</sub> /[M] <sub>aq,max</sub>	0.995 ± 5 × 10 <sup>-3</sup>	1	0.993	0.996	0.936
[M] <sub>IL</sub> /[M] <sub>IL,max</sub>	2.6 × 10 <sup>-3</sup> ± 7 × 10 <sup>-5</sup>	5.7 × 10 <sup>-3</sup>	4.9 × 10 <sup>-3</sup>	0.010	0.085
K				0.010	0.091
ΔG° (kJ mol <sup>-1</sup> )				12.31	6.50
temp (°C)	53.1	53.8	54.4	56.8	65.0
[M] <sub>aq</sub> /[M] <sub>aq,max</sub>	0.687	0.285 ± 3 × 10 <sup>-4</sup>	0.156	3.0 × 10 <sup>-3</sup>	4 × 10 <sup>-4</sup> ± 3 × 10 <sup>-6</sup>
[M] <sub>IL</sub> /[M] <sub>IL,max</sub>	0.360	0.736 ± 9 × 10 <sup>-3</sup>	0.909	0.980	1 ± 0.066
K	0.525	2.58	5.81	326	
ΔG° (kJ mol <sup>-1</sup> )	1.75	-2.58	-4.79	-15.87	

<sup>a</sup> Typical errors of the micelle concentrations are obtained from measurements on three separate samples for each datum. All of the samples are measured three times, and average values are reported.

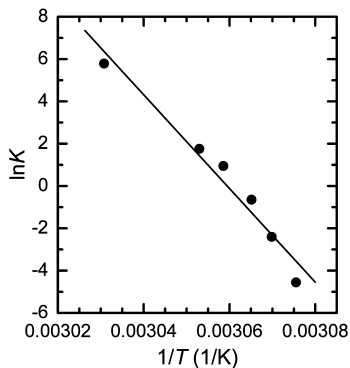


**Figure 3.** Equilibrium constant versus inverse temperature. The solid line is a linear fit with a correlation coefficient (*R*) of 0.981.

standard enthalpy change (ΔH°), and standard entropy change (ΔS°) of the transfer were calculated by<sup>32</sup>

$$\Delta G^\circ = -RT \ln K \quad (3)$$

$$\Delta H^\circ = -R \left[ \frac{\partial \ln K}{\partial (1/T)} \right]_P \quad (4)$$

$$\Delta S^\circ = \frac{\Delta H^\circ - \Delta G^\circ}{T} \quad (5)$$

where *R* is the gas law constant, *T* is the absolute temperature, and [∂ln *K*/∂(1/*T*)]<sub>P</sub> is the slope of the plot of natural log *K* versus the inverse of temperature (Figure 3). The calculated values of ΔG° are listed in Table 2, and those of ΔH° and ΔS° are 2 × 10<sup>3</sup> kJ mol<sup>-1</sup> and 6 × 10<sup>3</sup> J K<sup>-1</sup> mol<sup>-1</sup> (per mole of micelles), respectively, for the temperature range from 52.0 to 56.8 °C, where the dye concentrations are linearly related to the fluorescence intensities.

Since the driving force of the micelle shuttle arises from the solvated PEO corona block, the transfer can be described as a process of exchange of water and ionic liquid in the PEO corona. Therefore, the ΔH° and ΔS° can be written as

$$\Delta H^\circ = \Delta H^\circ_{\text{PEO-IL}} - \Delta H^\circ_{\text{PEO-water}} \quad (6)$$

$$\Delta S^\circ = \Delta S^\circ_{\text{PEO-IL}} - \Delta S^\circ_{\text{PEO-water}} \quad (7)$$

respectively, where ΔH°<sub>PEO-water</sub> and ΔS°<sub>PEO-water</sub> are the enthalpy and entropy changes of the formation of the interaction between the PEO corona and water, respectively, and ΔH°<sub>PEO-IL</sub>

and ΔS°<sub>PEO-IL</sub> are the enthalpy and entropy changes of the formation of the interaction between the PEO corona and [EMIM][TFSI], respectively. The positive values of ΔH° and ΔS° indicate that the dissolution of PEO in water is more energetically favorable but more entropy unfavorable than that in [EMIM][TFSI], and that the transfer is driven by entropy. Due to the hydrogen bond formation ability of the ether oxygen of PEO, hydrogen bonding is a significant factor in PEO dissolution. The LCST phase behavior of PEO in water was previously explained by a negative ΔH°<sub>PEO-water</sub> value, arising from the hydrogen bonding between PEO and water, and a negative ΔS°<sub>PEO-water</sub> value, arising from solvent structuring of PEO via the hydrogen bonding.<sup>33</sup> Watanabe et al. recently reported the LCST phase behavior of a PEO derivative, poly(ethyl glycidyl ether), in [EMIM][TFSI]; it is attributable to the hydrogen bonding between the imidazolium ring and the PEO derivative.<sup>34</sup> The hydrogen bonding was also supported by the report of Armstrong et al. where the hydrogen bond basicity of an imidazolium type ionic liquid is greatly enhanced upon adding Brij surfactants containing EO units.<sup>9b</sup> Zheng et al. recently reported that micellization of Pluronic poly(ethylene oxide)-poly(propylene oxide)-poly(ethylene oxide) (PEO-PPO-PEO) block copolymers in imidazolium ionic liquids has positive standard enthalpy and entropy changes, indicating an entropy-driven process.<sup>11a</sup> These results suggest that PEO possibly has similar hydrogen bonding with [EMIM][TFSI] and the solvent structuring effect, which would indicate negative ΔH°<sub>PEO-IL</sub> and ΔS°<sub>PEO-IL</sub> values. Quantitatively, the values of ΔH° and ΔS° are very large. This is not surprising because the values are per mole of micelles. The number of EO units in the PEO corona blocks of each micelle is estimated to be about 30 000.<sup>35</sup> Thus, the ΔH° and ΔS° per mole of EO units are much more modest, 0.06 kJ mol<sup>-1</sup> and 0.2 J K<sup>-1</sup> mol<sup>-1</sup>, respectively. It is possible that these values are reduced by the presence of water in the ionic liquid phase and [EMIM][TFSI] in the aqueous phase,<sup>36</sup> which could influence the interaction between PEO and the two solvents.<sup>24</sup>

**Micelle Transfer from Water to [EMIM][TFSI] under Quiescent Conditions.** Figure 4 shows experimental images for the transfer of dye-loaded micelles from water to [EMIM][TFSI] under quiescent conditions, after heating to 80 °C. On the basis of the experimental observations, the transfer takes place in three distinct steps. The first step is formation of micelle-concentrated [EMIM][TFSI] droplets in the water phase, shown by the first five images in Figure 4. Upon heating, the water phase gradually turns cloudy, indicating formation of large aggregates. The aggregates are proposed to be micelle-concentrated [EMIM][TFSI] droplets, since water is replaced

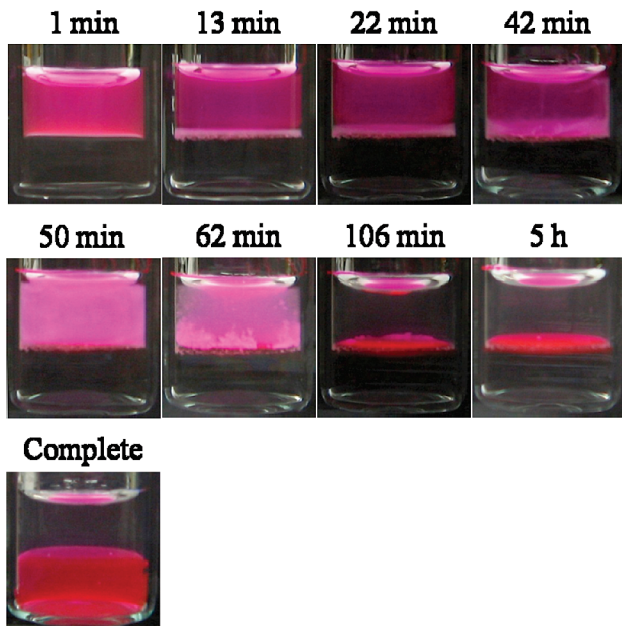


**Figure 4.** Transfer of the dye-loaded micelles from water to [EMIM][TFSI] under quiescent conditions upon heating at 80 °C. Both phases have a volume of 1 mL and a height of ~0.7 cm.

by [EMIM][TFSI] to solvate the PEO corona of the micelles in the transfer (see below for more discussion). The small amount of [EMIM][TFSI] in the water phase can assist the droplet formation; however, diffusion of [EMIM][TFSI] from the interface into the water phase is necessary to provide “extra” [EMIM][TFSI] for the droplets. This inference is supported by the observation that the interface is always the first place to turn cloudy, due to more abundant [EMIM][TFSI], and that the cloudiness gradually extends throughout the water phase, as shown in Figure 4.

To obtain a sense of the diffusion rate of [EMIM][TFSI] in the water phase, the mutual diffusion coefficient ( $D_m$ ) of [EMIM][TFSI] in water is estimated to be  $\sim 3 \times 10^{-9} \text{ m}^2 \text{ s}^{-1}$  at 80 °C, based on reported results.<sup>37</sup> The time ( $t$ ) for [EMIM][TFSI] to diffuse a mean square distance from the interface into the water phase can be calculated using the equation<sup>38</sup>

$$t = \frac{\overline{x^2}}{2D_m} \quad (8)$$

For example, it takes  $\sim 10$  min for [EMIM][TFSI] to diffuse 0.3 cm from the interface into the water phase.

The second step is sedimentation of the micelle-concentrated [EMIM][TFSI] droplets to the interface, shown by the fifth through the seventh images in Figure 4. The sedimentation originates from the density difference between the droplets and water; [EMIM][TFSI] has a density of 1.52 g/mL,<sup>39</sup> leading to a higher density of the droplets than water. Assuming the droplets are spherical, their size can be estimated by the equation<sup>38</sup>

$$R_d = \left( \frac{9\nu}{2(\rho_2 - \rho_1)g} \right)^{0.5} \quad (9)$$

where  $R_d$  is the radius of the droplets,  $\eta$  is the viscosity of the solvent,  $\nu$  is the speed of sedimentation,  $\rho_1$  and  $\rho_2$  are the densities of the solvent and the droplets, respectively, and  $g$  is the acceleration of gravity. From the observation of the sedimentation

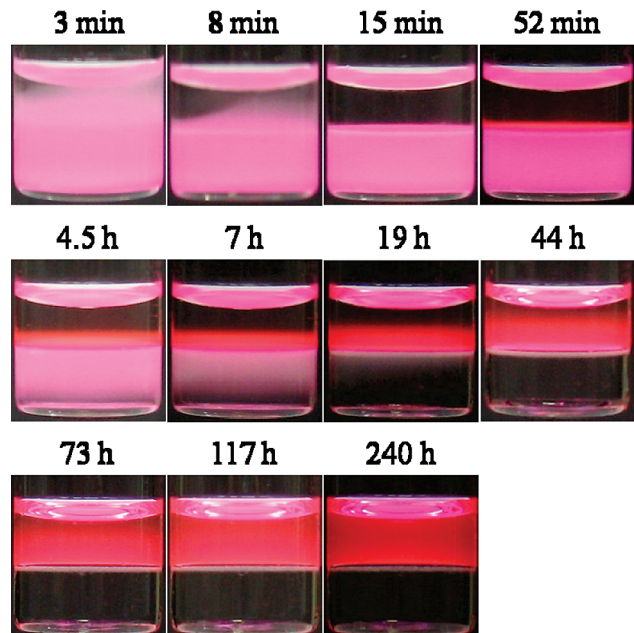


**Figure 5.** Transfer of the dye-loaded micelles from [EMIM][TFSI] to water under quiescent conditions, after cooling the final system in Figure 4 from 80 to 22 °C. Both phases have a volume of 1 mL and a height of ~0.7 cm.

process,  $\nu$  is about  $3 \times 10^{-6} \text{ m s}^{-1}$ . If the density of pure [EMIM][TFSI] is used as  $\rho_2$ ,  $R_d$  is calculated to be about 1  $\mu\text{m}$ . The size is underestimated, because the actual  $\rho_2$  should be lower than the density of [EMIM][TFSI], as the block copolymer in the droplets has a lower density than [EMIM][TFSI].<sup>26</sup> The size of the droplets is significantly larger than that of the micelles forming the droplets, which have a mean hydrodynamic radius ( $\langle R_h \rangle$ ) of 27 nm and a reduced second cumulant ( $\mu_2/\Gamma^2$ ) of 0.18, which is a measure of the width of micelle size distribution,<sup>40</sup> as determined by DLS. For dilute solutions,  $D_m$  and  $R_h$  are related by the Stokes–Einstein equation<sup>38</sup>

$$R_h = \frac{kT}{6\pi\eta D_m} \quad (10)$$

where  $k$  is the Boltzmann constant. A micrometer size scale for the droplets is consistent with the cloudy appearance of the water phase and the sedimentation of the droplets.

The third step is diffusion of the micelles from the interface into the ionic liquid phase, shown by the last three images in Figure 4. The  $D_m$  of the micelles is  $1.2 \times 10^{-12} \text{ m}^2 \text{ s}^{-1}$  in [EMIM][TFSI] at 80 °C, so by eq 8, the diffusion step should take about 2 months. However, it is difficult to follow the diffusion process for such a long time at that relatively high temperature.<sup>41</sup> An analogous process, diffusion of the micelles from the interface into the water phase, will be discussed below and provide more information about this step.

The micelle transfer from water to [EMIM][TFSI] under quiescent conditions was also performed at 65 °C. In comparison with the transfer at 80 °C, it took longer for the water phase to turn cloudy and for the droplets to sediment to the interface, and the water phase is less cloudy. These observations indicate slower kinetics and a smaller droplet size at the lower temperature.

**Micelle Transfer from [EMIM][TFSI] to Water under Quiescent Conditions.** Figure 5 shows experimental images of the micelle transfer from [EMIM][TFSI] to water under

quiescent conditions, upon cooling the final system in Figure 4 to room temperature. Similarly, on the basis of the observation of the images, the transfer can also be resolved into three steps. The first step is the formation of [EMIM][TFSI] droplets in the water phase, in addition to water droplets and micelle-concentrated water droplets in the ionic liquid phase, as shown by the first image in Figure 5. The formation of the water droplets and the [EMIM][TFSI] droplets is due to the decreasing miscibility of water and [EMIM][TFSI] upon cooling.<sup>36</sup> This can be directly visualized by the cloudy appearance of both the water and ionic liquid phases in the biphasic system without micelles. The “extra” water can assist the formation of the micelle-concentrated water droplets, in which [EMIM][TFSI] is replaced by water to solvate the PEO corona of the micelles. The second step is sedimentation of the [EMIM][TFSI] droplets, as well as creaming of the water droplets and the micelle-concentrated water droplets to the interface, as shown by the first seven images in Figure 5. The sedimentation and creaming are likewise due to density differences. The observed sedimentation and creaming rates are about  $1 \times 10^{-5}$  and  $2 \times 10^{-7} \text{ m s}^{-1}$ , respectively, and therefore, the sizes of the [EMIM][TFSI] droplets in water as well as the micelle-concentrated water droplets (and perhaps the water droplets) in the ionic liquid can be calculated by eq 9; they have similar values of  $R_d$ , about 3  $\mu\text{m}$ . The much lower creaming speed than the sedimentation speed is mainly because [EMIM][TFSI] has an  $\sim 40$  times higher viscosity than water.<sup>17</sup> The third step is diffusion of the micelles to the water phase, as shown by the 3rd through the 11th images in Figure 5. The diffusion process is also very slow and takes about 10 days to complete. By eq 8, the  $D_m$  of the micelles in the water phase is estimated to be  $7 \times 10^{-12} \text{ m}^2 \text{ s}^{-1}$ , which is consistent with the value,  $9 \times 10^{-12} \text{ m}^2 \text{ s}^{-1}$ , measured directly by DLS.

Micelle transfer from [EMIM][TFSI] to water under quiescent conditions was also performed by adding water to a dry [EMIM][TFSI] solution of the micelles at room temperature (Figure S5 in the Supporting Information). This transfer is similar to the micelle transfer in Figure 5 yet different in that, at the beginning, the ionic liquid phase is dry and therefore there are no water droplets in the ionic liquid phase and no [EMIM][TFSI] droplets in the water phase. Therefore, it is necessary for water to diffuse from the interface to saturate the ionic liquid phase and replace [EMIM][TFSI] to solvate the PEO corona of the micelles. This is analogous to the first step of the micelle transfer from water to [EMIM][TFSI] at high temperature above, but it takes longer due to the higher viscosity of [EMIM][TFSI].

**Mechanism of the Micelle Shuttle.** On the basis of the results above, a mechanism is proposed for the micelle shuttle under quiescent conditions (Figure 6). There are three steps in the micelle transfer from the water phase to the ionic liquid phase upon heating. First, micelle-concentrated ionic liquid droplets form in the water phase, since water is replaced by the ionic liquid to solvate the PEO corona of the micelles. The “extra” (more than saturated) ionic liquid for the droplet formation in the water phase is provided by the diffusion of the ionic liquid from the interface into the water phase. Second, the micelle-concentrated ionic liquid droplets sediment to the interface due to their higher density. Finally, the micelles diffuse from the interface into the ionic liquid phase. Similarly, there are also three steps in the reverse transfer upon cooling the micelle shuttle system equilibrated at high temperature. First, due to the decreasing miscibility of water and the ionic liquid upon cooling, the water droplets and the ionic liquid droplets

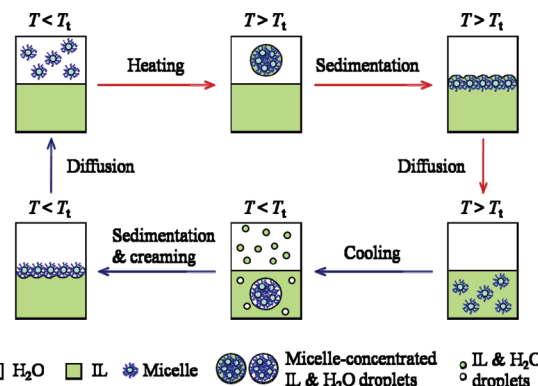


**Figure 6.** Schematic illustration of the mechanism of the micelle shuttle. Micelles and droplets are not drawn to scale.

are formed immediately in the ionic liquid phase and the water phase, respectively. The “extra” water in the ionic liquid phase facilitates the formation of the micelle-concentrated water droplets, in which the ionic liquid is replaced by water to solvate the PEO corona of the micelles. Second, all of the droplets sediment or cream to the interface due to density differences. Finally, the micelles diffuse from the interface into the water phase.

For applications, the slow kinetics of the micelle shuttle can be significantly accelerated by using thin fluid layers and/or by vigorous stirring, whereby the diffusion, sedimentation, and creaming proceed much more rapidly. For example, with only moderate stirring, both of the transfers can be completed within 1 h.

## Conclusion

We have demonstrated a dye-loaded block copolymer micelle shuttle for transportation between water and an ionic liquid. The round-trip transportation of a high molar absorption and quantum yield dye is fully thermoreversible, quantitative, and without leakage. Quantitative fluorescence analysis reveals a very strong temperature dependence of the micelle distribution in the biphasic system, which is quite favorable for controlled round-trip quantitative transportation by the micelle shuttle.

The temperature dependence of the micelle distribution was used to extract thermodynamic variables of the micelle transfer,  $\Delta G^\circ$ ,  $\Delta H^\circ$ , and  $\Delta S^\circ$ . Both  $\Delta H^\circ$  and  $\Delta S^\circ$  are positive, indicating an entropy-driven transfer. This is consistent with common entropy-driven phase transitions of polymers in water. The values of  $\Delta H^\circ$  and  $\Delta S^\circ$  are very large, which leads to the strong temperature dependence of the micelle distribution. This is because the number of EO monomer units, which provide the driving force of the micelle transfer, is tens of thousands in each micelle. To understand the transfer kinetics, the micelle shuttle was studied under quiescent conditions. This also sheds light on the interesting phenomenon that the micelles in a phase can “feel” the solvent far away in the other phase and “respond” spontaneously to transfer. It is found that both two-way transfers involve three steps, formation of micelle-concentrated [EMIM][TFSI]/water droplets in the initial phase, sedimentation/creaming of the droplets to the interface, and diffusion of the micelles to the destination phase. A transfer mechanism is thus proposed for the micelle shuttle.

**Acknowledgment.** This work was supported by the National Science Foundation through Awards DMR-0406656 and DMR-0804197. We acknowledge Dr. Kevin P. Davis for generous supply of the block copolymer and Prof. Valerie C. Pierre for

providing access to the UV-visible and fluorescence spectrophotometers.

**Supporting Information Available:** MALDI spectra of PB and Rho-PB. Visible spectra of rhodamine B base, Rho-PB, and Rho-PB-loaded PB-PEO micelles in water and [EMIM][TFSI]. Fluorescence spectra of dye-loaded micelles in water and [EMIM][TFSI]. Dependence of fluorescence intensity on the concentration of Rho-PB. Micelle transfer from [EMIM][TFSI] to water under quiescent conditions upon adding water to a dry [EMIM][TFSI] solution of the dye-loaded micelles at room temperature. This material is available free of charge via the Internet at <http://pubs.acs.org>.

## References and Notes

- (1) (a) Allen, C.; Maysinger, D.; Eisenberg, A. *Colloids Surf., B* **1999**, *16*, 3–27. (b) Savic, R.; Luo, L. B.; Eisenberg, A.; Maysinger, D. *Science* **2003**, *300*, 615–618. (c) Lodge, T. P.; Rasdal, A.; Li, Z.; Hillmyer, M. A. *J. Am. Chem. Soc.* **2005**, *127*, 17608–17609.
- (2) Alexandridis, P.; Lindman, B., Eds. *Amphiphilic Block Copolymers: Self-Assembly and Applications*; Elsevier: Amsterdam, The Netherlands, 2000.
- (3) (a) Vriezema, D. M.; Aragones, M. C.; Elemans, J. A. A. W.; Cornelissen, J. J. L. M.; Rowan, A. E.; Nolte, R. J. M. *Chem. Rev.* **2005**, *105*, 1445–1489. (b) Dwars, T.; Paetzold, E.; Oehme, G. *Angew. Chem., Int. Ed.* **2005**, *44*, 7174–7199.
- (4) (a) Bates, F. S.; Fredrickson, G. H. *Phys. Today* **1999**, *52*, 32–38. (b) Lodge, T. P. *Macromol. Chem. Phys.* **2003**, *204*, 265–273.
- (5) (a) Hawker, C. J.; Wooley, K. L. *Science* **2005**, *309*, 1200–1205. (b) Won, Y. Y.; Brannan, A. K.; Davis, H. T.; Bates, F. S. *J. Phys. Chem. B* **2002**, *106*, 3354–3364. (c) Davis, K. P.; Lodge, T. P.; Bates, F. S. *Macromolecules* **2008**, *41*, 8289–8291. (d) Li, Z.; Kesselman, E.; Talmon, Y.; Hillmyer, M. A.; Lodge, T. P. *Science* **2004**, *306*, 98–101. (e) Gil, E. S.; Hudson, S. M. *Prog. Polym. Sci.* **2004**, *29*, 1173–1222.
- (6) (a) Zhang, L.; Yu, K.; Eisenberg, A. *Science* **1996**, *272*, 1777–1779. (b) Zhang, L.; Eisenberg, A. *Macromolecules* **1999**, *32*, 2239–2249. (c) Cui, H. G.; Chen, Z. Y.; Zhong, S.; Wooley, K. L.; Pochan, D. J. *Science* **2007**, *317*, 647–650. (d) Bang, J.; Jain, S.; Li, Z.; Lodge, T. P.; Pedersen, J. S.; Kesselman, E.; Talmon, Y. *Macromolecules* **2006**, *39*, 1199–1208. (e) Liu, C.; Hillmyer, M. A.; Lodge, T. P. *Langmuir*, ASAP.
- (7) (a) Welton, T. *Chem. Rev.* **1999**, *99*, 2071–2083. (b) Han, X.; Armstrong, D. W. *Acc. Chem. Res.* **2007**, *40*, 1079–1086. (c) Rogers, R. D., Seddon, K. R., Eds. *Ionic liquids IIIA: Fundamentals, Progress, Challenges, and Opportunities Properties and Structure*; ACS Symposium Series 901; American Chemical Society: Washington, DC, 2005. (d) Rogers, R. D., Seddon, K. R., Eds. *Ionic liquids IIIB: Fundamentals, Progress, Challenges, and Opportunities Transformations and Processes*; ACS Symposium Series 902; American Chemical Society: Washington, DC, 2005.
- (8) Greaves, T. L.; Drummond, C. J. *Chem. Soc. Rev.* **2008**, *37*, 1709–1726.
- (9) (a) Evans, D. F.; Yamauchi, A.; Roman, R.; Casassa, E. Z. *J. Colloid Interface Sci.* **1982**, *88*, 89–96. (b) Anderson, J. L.; Pino, V.; Hagberg, E. C.; Sheares, V. V.; Armstrong, D. W. *Chem. Commun.* **2003**, 2444–2445. (c) Fletcher, K. A.; Pandey, S. *Langmuir* **2004**, *20*, 33–36. (d) Hao, J.; Song, A.; Wang, J.; Chen, X.; Zhuang, W.; Shi, F.; Zhou, F.; Liu, W. *Chem.—Eur. J.* **2005**, *11*, 3936–3940. (e) Li, N.; Zhang, S.; Zheng, L.; Wu, J.; Li, X.; Li, Y. *J. Phys. Chem. B* **2008**, *112*, 12453–12460.
- (10) (a) He, Y.; Li, Z.; Simone, P. M.; Lodge, T. P. *J. Am. Chem. Soc.* **2006**, *128*, 2745–2750. (b) Simone, P. M.; Lodge, T. P. *Macromolecules* **2008**, *41*, 1753–1759. (c) Ueki, T.; Watanabe, M.; Lodge, T. P. *Macromolecules* **2009**, *42*, 1315–1320. (d) Meli, L.; Lodge, T. P. *Macromolecules* **2009**, *42*, 580–583. (e) He, Y.; Lodge, T. P. *Chem. Commun.* **2007**, 2732–2734. (f) Noro, A.; Matsushita, Y.; Lodge, T. P. *Macromolecules* **2008**, *41*, 5839–5844. (g) Lee, J.; Panzer, M. J.; He, Y.; Lodge, T. P.; Frisbie, C. D. *J. Am. Chem. Soc.* **2007**, *129*, 4532–4533. (h) Noro, A.; Matsushita, Y.; Lodge, T. P. *Macromolecules* **2009**, *42*, 5802–5810.
- (11) (a) Zhang, S.; Li, N.; Zheng, L.; Li, X.; Gao, Y.; Yu, L. *J. Phys. Chem. B* **2008**, *112*, 10228–10233. (b) Tamura, S.; Ueki, T.; Ueno, K.; Kodama, K.; Watanabe, M. *Macromolecules* **2009**, *42*, 6239–6244. (c) Virgili, J. M.; Hexemer, A.; Pople, J. A.; Balsara, N. P.; Segalman, R. A. *Macromolecules* **2009**, *42*, 5642–5651.
- (12) (a) Ueki, T.; Watanabe, M. *Macromolecules* **2008**, *41*, 3739–3749. (b) Lodge, T. P. *Science* **2008**, *321*, 50–51.
- (13) Ueki, T.; Watanabe, M. *Langmuir* **2007**, *23*, 988–990.
- (14) Ueki, T.; Watanabe, M. *Chem. Lett.* **2006**, *35*, 964–965.
- (15) He, Y.; Lodge, T. P. *J. Am. Chem. Soc.* **2006**, *128*, 12666–12667.
- (16) (a) Won, Y. Y.; Davis, H. T.; Bates, F. S. *Macromolecules* **2003**, *36*, 953–955. (b) Jain, S.; Bates, F. S. *Macromolecules* **2004**, *37*, 1511–1523.
- (17) Bai, Z.; He, Y.; Lodge, T. P. *Langmuir* **2008**, *24*, 5284–5290.
- (18) Bai, Z.; He, Y.; Young, N. P.; Lodge, T. P. *Macromolecules* **2008**, *41*, 6615–6617.
- (19) Guerrero-Sanchez, C.; Gohy, J. F.; D'Haese, C.; Thijs, H.; Hoogenboom, R.; Schubert, U. S. *Chem. Commun.* **2008**, 2753–2755.
- (20) (a) Chechik, V.; Zhao, M.; Crooks, R. M. *J. Am. Chem. Soc.* **1999**, *121*, 4910–4911. (b) Tian, H.; Chen, X.; Lin, H.; Deng, C.; Zhang, P.; Wei, Y.; Jing, X. *Chem.—Eur. J.* **2006**, *12*, 4305–4312. (c) Marcilla, R.; Curri, M. L.; Cozzoli, P. D.; Martinez, M. T.; Loinaz, I.; Grande, H.; Pomposo, J. A.; Mecerreyres, D. *Small* **2006**, *2*, 507–512. (d) Li, D.; Zhao, B. *Langmuir* **2007**, *23*, 2208–2217.
- (21) Dupont, J.; de Souza, R. F.; Suarez, P. A. Z. *Chem. Rev.* **2002**, *102*, 3667–3692.
- (22) (a) Eastoe, J.; Gold, S.; Rogers, S. E.; Paul, A.; Welton, T.; Heenan, R. K.; Grillo, I. *J. Am. Chem. Soc.* **2005**, *127*, 7302–7303. (b) Gao, Y.; Han, S.; Han, B.; Li, G.; Shen, D.; Li, Z.; Du, J.; Hou, W.; Zhang, G. *Langmuir* **2005**, *21*, 5681–5684. (c) Liu, J. H.; Cheng, S. Q.; Zhang, J. L.; Feng, X. Y.; Fu, X. G.; Han, B. X. *Angew. Chem., Int. Ed.* **2007**, *46*, 3313–3315. (d) Gao, Y.; Li, N.; Zheng, L.; Bai, X.; Yu, L.; Zhao, X.; Zhang, J.; Zhao, M.; Li, Z. *J. Phys. Chem. B* **2007**, *111*, 2506–2513.
- (23) (a) Merrigan, T. L.; Bates, E. D.; Dorman, S. C.; Davis, J. H. *Chem. Commun.* **2000**, 2051–2052. (b) Nakashima, T.; Kimizuka, N. *J. Am. Chem. Soc.* **2003**, *125*, 6386–6387. (c) Binks, B. P.; Dyab, A. K. F.; Fletcher, P. D. I. *Chem. Commun.* **2003**, 2540–2541.
- (24) Reichardt, C. *Green Chem.* **2005**, *7*, 339–351.
- (25) Du, H.; Fuh, R. A.; Li, J.; Corkan, A.; Lindsey, J. S. *Photochem. Photobiol.* **1998**, *68*, 141–142.
- (26) Fetter, L. J.; Lohse, D. J.; Richter, D.; Witten, T. A.; Zirkel, A. *Macromolecules* **1994**, *27*, 4639–4647.
- (27) Hillmyer, M. A.; Bates, F. S. *Macromolecules* **1996**, *29*, 6994–7002.
- (28) Susan, M. A. B. H.; Kaneko, T.; Noda, A.; Watanabe, M. *J. Am. Chem. Soc.* **2005**, *127*, 4976–4983.
- (29) Dujols, V.; Ford, F.; Czarnik, A. W. *J. Am. Chem. Soc.* **1997**, *119*, 7386–7387.
- (30) Zettl, H.; Hafner, W.; Boker, A.; Schmalz, H.; Lanzendorfer, M.; Muller, A. H. E.; Krausch, G. *Macromolecules* **2004**, *37*, 1917–1920.
- (31) Normalized micelle concentrations are used because the micelle concentrations are obtained from the fluorescence intensity of THF solutions containing the aqueous phase or the ionic liquid phase, and thus, there is ~7% water or [EMIM][TFSI] in the THF solutions (see the Experimental Section), which might affect the molar absorptivity and quantum yield of the dye.
- (32) Berry, R. S.; Rice, S. A.; Ross, J. *Physical Chemistry*; Oxford University Press: New York, 2000.
- (33) Kjellander, R.; Florin, E. J. *Chem. Soc., Faraday Trans. 1* **1981**, *77*, 2053–2077.
- (34) Tsuda, R.; Kodama, K.; Ueki, T.; Kokubo, H.; Imabayashi, S.; Watanabe, M. *Chem. Commun.* **2008**, 4939–4941.
- (35) The aggregation number is calculated from the volume of the core domain and the PB bulk density using the method and corresponding results reported in refs 10a and 10d. The radius of the core domain is estimated to be ~9 nm, evaluated from its relation with the composition of the block copolymer and the mean hydrodynamic radius of the micelles (27 nm).
- (36) Freire, M. G.; Carvalho, P. J.; Gardas, R. L.; Marrucho, I. M.; Santos, L. M. N. B. F.; Coutinho, J. A. P. *J. Phys. Chem. B* **2008**, *112*, 1604–1610. The solubility of [EMIM][TFSI] in water and water in [EMIM][TFSI] is 0.046 and 1.07 mmol/g, respectively, at room temperature.
- (37) Wong, C. L.; Soriano, A. N.; Li, M. H. *Fluid Phase Equilib.* **2008**, *271*, 43–52.
- (38) Hiemenz, P. C.; Rajagopalan, R. *Principles of Colloid and Surface Chemistry*; Marcel Dekker, Inc.: New York, 1997.
- (39) Bonhote, P.; Dias, A.-P.; Papageorgiou, N.; Kalyanasundaram, K.; Grätzel, M. *Inorg. Chem.* **1996**, *35*, 1168–1178.
- (40) Koppel, D. E. *J. Chem. Phys.* **1972**, *57*, 4814–4820.
- (41) Upon heating, ionic liquid droplets slowly form on the interface of water and air. The droplets accumulate and fall to the ionic liquid phase due to gravity, which leads to convection and hence accelerates the diffusion of the micelles in the ionic liquid phase.